Macromolecules

pubs.acs.org/Macromolecules

Article

Solvent Controls Nanoparticle Size during Nanoprecipitation by Limiting Block Copolymer Assembly

Giovanni Bovone, Lucien Cousin, Fabian Steiner, and Mark W. Tibbitt*

Cite This: *Macromolecules* 2022, 55, 8040–8048

Read Online

ACCESS | Metrics & More | Article Recommendations | Supporting Information

ABSTRACT: Control of the properties of nanoparticles (NPs), including size, is critical for their application in biomedicine and engineering. Polymeric NPs are commonly produced by nanoprecipitation, where a solvent containing a block copolymer is mixed rapidly with a nonsolvent, such as water. Empirical evidence suggests that the choice of solvent influences NP size; yet, the specific mechanism remains unclear. Here, we show that solvent controls NP size by limiting block copolymer assembly. In the initial stages of mixing, polymers assemble into dynamic aggregates that grow via polymer exchange. At later stages of mixing, further growth is prevented beyond a solvent-specific water fraction. Thus, the solvent sets NP size by controlling the extent of dynamic growth up to growth arrest. An *a priori* model based on spinodal decomposition corroborates our proposed mechanism, explaining how size scales with the solvent-dependent critical water fraction of growth arrest and enabling more efficient NP engineering.

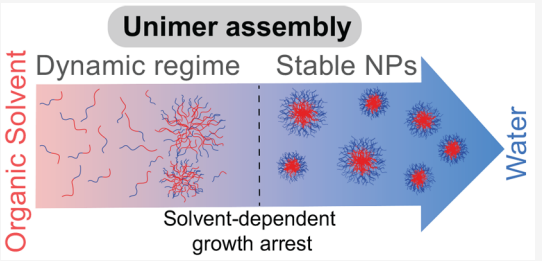

INTRODUCTION

Polymeric nanoparticles (NPs) are increasingly applied as colloidal drug delivery systems and building blocks in advanced (bio)material design.[1−6] Efficient translation of NPs and NP-based materials into clinical and industrial products requires strict control over the physicochemical properties of the engineered colloids, including NP size.[7−11] Nanoprecipitation is a robust method to produce NPs from amphiphilic block copolymers.[12−14] In a typical nanoprecipitation, a solution containing a water-miscible organic solvent and a block copolymer is mixed with a nonsolvent (water). Mixing induces a rapid change in solvent composition causing dynamic block copolymer aggregation as the solubility of the hydrophobic block decreases. The aggregates grow and mature into kinetically trapped (frozen) NPs with a hydrophobic core and a hydrophilic corona. The NPs become frozen as the low solubility of individual block copolymer chains (unimers) in the final mixture prevents further growth by unimer exchange and the hydrophilic corona inhibits NP fusion.[15] Thus, nanoprecipitation is a kinetic process, and NP size can be controlled by the mixing time scale, τ_{mix}.[16] The physicochemical properties of the formed NPs can be further influenced by the block constituents, block molecular weights, polymer concentrations, and the choice of solvent.[17−20]

Experimental evidence has highlighted that the solvent in which the precursor materials are dissolved affect NP size following nanoprecipitation.[20,21] Yet, there is no physical explanation for the specific role of the solvent.[15] Solvent composition was shown to regulate the shape and dynamics of aggregating block copolymers.[22−24] During nanoprecipitation of monolithic hydrophobic polymers, NP size correlated to the Hansen solubility parameter (HSP) distance, or solvent−water affinity, of the selected solvent.[25,26] Solvents with high water affinity and low viscosity improved solvent diffusion into the aqueous phase, forming smaller NPs based on the rapid rate of change in solvent quality, χ. For solid lipid NPs, size increased with solvent viscosity.[27,28] However, for the nanoprecipitation of amphiphilic block copolymers NP size does not scale with solvent−water affinity or solvent viscosity.[21] Despite the importance of the solvent in block copolymer nanoprecipitation, a physical relation between solvent properties and NP size is lacking.

The effect of the mixing kinetics on block copolymer nanoprecipitation has been described.[29] Pioneering work by Prud'homme and co-workers demonstrated that the mixing time scale, τ_{mix}, and polymer composition influence NP size, dispersity, and corona density.[16,30−33] In these studies, flow-based mixing devices controlled τ_{mix}.[34] The assembly and growth of block copolymers into NPs was modeled via Smoluchowski diffusion-limited growth kinetics. Unimer exchange and aggregate fusion enabled growth until a sufficient corona density was formed and the NPs became kinetically trapped (frozen). τ_{mix} influenced NP size as the rate of change in the solvent composition controlled the amount of time for

Received: May 16, 2022
Revised: July 20, 2022
Published: September 9, 2022

https://doi.org/10.1021/acs.macromol.2c00907
Macromolecules 2022, 55, 8040−8048

aggregate growth prior to NP freezing.[16,30,35,36] Evidence suggests that under intermediate solvent quality conditions self-assembly of block copolymers is preceded by liquid−liquid phase separation, and the dimensions of the initial polymer-rich liquid droplets influence the final aggregate size.[37−39] Drese and colleagues developed a computational model of nanoprecipitation to predict NP size based on τ_{mix} and a theoretical solvent with time-varying quality, $\chi(t)$.[40,41] In their computational model, an initial change in χ, upon mixing, induced spinodal decomposition and unimer aggregation. These aggregates grew via Ostwald ripening until they became kinetically trapped (frozen) at a critical solvent quality, χ_c. Here, χ_c was defined as a freezing point that prevented further unimer exchange or aggregate fusion. Thus, NP size was controlled by the rate of change in χ, governed by τ_{mix}, up to a critical set point, χ_c. These studies suggest a combined effect of mixing kinetics and solvent properties on NP size, but a relation to a measurable parameter of the selected solvent has not been shown.

Here, we investigate the specific role of the solvent on NP size during nanoprecipiation of block copolymers. Experimentally, we observed a significant influence of the choice of solvent on NP size. To explain this, we hypothesized that the solvent defines a measurable critical water fraction of growth arrest, ϕ_c, that is analogous to χ_c, beyond which further NP growth is prevented. Turbidity measurements confirmed that the block copolymer aggregates formed frozen NPs at ϕ_c for all solvents tested. NP size correlated to the measured ϕ_c and did not correlate with the HSP distance or solvent viscosity. In addition, the block copolymer assemblies were macroscopically dynamic below ϕ_c, enabling aggregation and growth up to this critical point. Thus, NP size was defined by the solvent choice and the mixing kinetics as the extent of growth was controlled by the time needed to reach the solvent-dependent ϕ_c. We observed a scaling behavior for NP size as a function of mixing kinetics, when NP size was scaled by the solvent-dependent ϕ_c. An *a priori* scaling model described the specific role of the solvent based on spinodal decomposition, growth by unimer exchange, and freezing of the NPs at the solvent-dependent point of growth arrest. In this model, the solvent controls NP size by setting ϕ_c, and the mixing kinetics dictate the rate at which the system reaches this freezing point. Our study offers fundamental insight into the role of the solvent on NP size during nanoprecipitation, and this understanding will enable more efficient engineering of this important class of materials.

MATERIALS AND METHODS

Materials. Chemical reagents and solvent were purchased from Sigma-Aldrich or VWR and used as received unless otherwise noted. Poly(ethylene glycol)$_{5kDa}$-*block*-poly(DL-lactide)$_{20kDa}$ (PEG-*b*-PLA), PEG$_{5kDa}$-*b*-poly(lactide-*co*-glycolide)$_{20kDa}$ (PEG-*b*-PLGA), and PEG$_{5kDa}$-*b*-polycaprolactone$_{20kDa}$ (PEG-*b*-PCL) were purchased from Akina PolySciTech (USA). Deionized water was generated with a Millipore Milli-Q system and Biopak filter. All microfluidic components were purchased from BGB Analytics unless stated otherwise.

Dynamic Light Scattering. The hydrodynamic diameter, D_h, and dispersity, $Đ$, of the nanoparticles were measured via dynamic light scattering (DLS; Malvern ZetaSizer Nano ZS). DLS measurements were collected in a polystyrene semi-microcuvette (path length ∼10 mm) at a scattering angle of 173° and at a temperature of 25 °C. D_h and $Đ$ were taken as the respective *z*-average and the dispersity index of the NP intensity distribution. Unless stated otherwise, the NP size reported corresponds to D_h and $Đ$ which were calculated from the average of three DLS measurements per sample.

Transmission Electron Microscopy (TEM). TEM pictures were taken of a FEI Morgagni 268 (Thermo Fisher) instrument at an acceleration of 100 kV. Samples were prepared on a 200-mesh Formvar and carbon-coated copper grids (Quantifoil Micro Tools GmbH) which were glow-discharged with negative polarity for 30 s (EMITECH K100X; Quorum Technologies). The treated grids were placed upside down for 2 min onto 50 μL of nanoparticle suspension to promote particle adsorption on the grids. The residual liquid was subsequently blotted away with filter paper, and the grid was negatively stained for 15 s with 2% w/v uranyl acetate aqueous solution by adopting the same blotting procedure. The residual moisture present on the grid was dried in air prior to imaging.

Batch Nanoprecipitation. Block copolymer solutions were prepared by dissolving polymer (2.5−10 mg mL^{-1}; PEG-*b*-PLA, PEG-*b*-PLGA, or PEG-*b*-PCL) in a water-miscible organic solvent (DMF, acetone, acetonitrile, THF, or DMSO). Batch nanoprecipitation was performed by adding the block copolymer solution dropwise (∼25 μL per drop) to deionized water (10 mL) in a 20 mL scintillation vial under vigorous stirring (650 rpm; Heidolph MR Hei-Tec; 15 mm Teflon-coated stir bar). The solvent−water ratio, *R*, was defined as $R = \frac{V_{solvent}}{V_{water}}$. The batch nanoprecipitations were performed with R = 0.005. The NP size (D_h) and dispersity ($Đ$) were measured via DLS. All experiments were performed in triplicate.

Turbidity Measurements. The block copolymers were dissolved in each of the water-miscible organic solvents (4 or 10 mg mL^{-1}). The measurements were directly performed in disposable Brand Micro Cuvettes. Deionized water was titrated sequentially to increase the water fraction in the solution (volumetric fraction of water; v/v) and pipetted for ∼3 s prior to starting the turbidity measurement. The turbidity was measured on a PerkinElmer Lambda 35 UV−vis spectrophotometer (λ_{abs} = 500 nm). Rayleigh scattering of the polymer aggregates should have occurred when the objects were larger than $\lambda/20$ (∼25 nm).[42] The water fraction was increased in 0.02 steps from 0.0 to 0.5 or until further changes in turbidity upon water addition were negligible.

To investigate the reversibility of block copolymer assembly, an analogous procedure was used to reduce the water fraction. The water fraction was decreased in 0.02 steps by sequentially adding a solution of block copolymer dissolved in the related organic solvent (4 or 10 mg mL^{-1}). The measurement was performed as described above where after each addition the suspension was mixed for ∼3 s and solution turbidity was measured. The addition of polymer solution was stopped when further changes in suspension turbidity were negligible.

During dynamic turbidity measurements, the suspension turbidity was monitored over time. Water or block copolymer solution was titrated as mentioned above. Upon each stepwise change of water fraction the suspension turbidity was monitored every second over 10−60 min until stabilization occurred.

Experimental Determination of ϕ_c. The critical water fraction of growth arrest, ϕ_c, was determined for each solvent−block copolymer pair from the respective turbidity measurements. ϕ_c represented the water fraction at which the turbidity plateaued after the turbidity maximum. The value of ϕ_c was defined as the lowest concentration of water at which the turbidity was ±20% of the final plateau (last four points). DMSO did not have a turbidity maximum; therefore, the threshold of deviation from the plateau was set to ±10%.

Coaxial Jet Mixer Nanprecipitation. The coaxial jet mixer CJM was developed based on studies published previously by our group.[14] The device consisted of two coaxial tubes, through which the polymer solution (inner fused silica tube) and water (outer PTFE tube) flowed. Flow was controlled with two CETONI NeMESYS syringe pumps and the related software Qmix elements (CETONI GmbH). The polymer solutions and water were injected with SETonic gastight syringes with volumes ranging from 0.5 to 50 mL. Syringe outlets were connected to PTFE tubes [outer diameter, OD: 1587 μm; inner

https://doi.org/10.1021/acs.macromol.2c00907
Macromolecules 2022, 55, 8040−8048

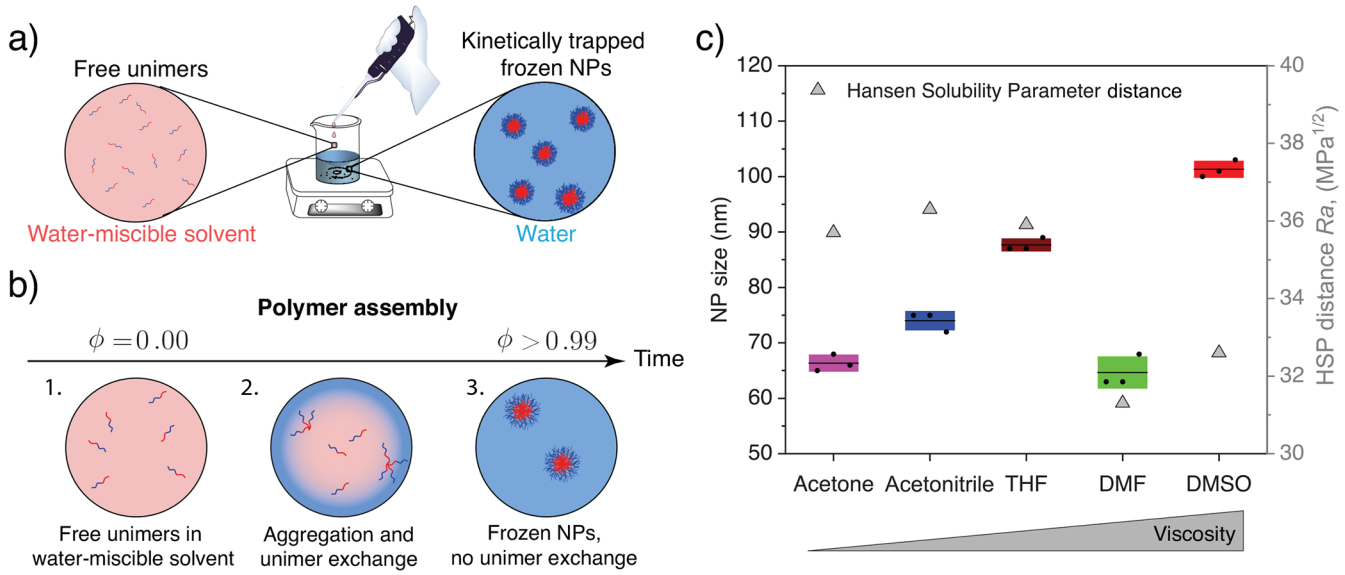

Figure 1. Solvent choice controls NP size. (a) During batch nanoprecipitation, a NP precursor solution containing a block copolymer dissolved in a water-miscible organic solvent is added dropwise to water under vigorous stirring. Rapid mixing of the block copolymer solution with water triggers polymer assembly and, ultimately, the formation of kinetically trapped (frozen) NPs. (b) The polymer assembly process proceeds in three steps: (1) Block copolymers are dissolved in a favorable solvent. (2) Solvent mixing with water alters the local solvent quality, χ. The change in χ triggers block copolymer assembly into dynamic aggregates, which can grow via unimer exchange or aggregate fusion. (3) A rise in water fraction increases the energy barrier for unimer exchange and fusion. Growth arrest occurs at a critical solvent quality, χ_c, forming kinetically trapped core−shell NPs. (c) The size of PEG-*b*-PLA NPs following nanoprecipitation with common solvents varied with the choice of solvent (5 mg mL^{-1} PEG-*b*-PLA; R = 0.005). NP size did not correlate with solvent viscosity (solvents are plotted in order of increasing viscosity) or the Hansen solubility parameter (HSP) distance, *Ra* (gray triangles), calculated between the solvent and water (Supporting Information Section S2). Data are plotted as mean (black line) ± SD (colored box) for three independent experiments (black circles).

diameter, ID: 793 μm; Cole-Parmer, USA]. The tube connected to the polymer solution syringe was further attached to a fused silica capillary (OD: 363 μm, ID: 100 μm, length (L): 7 cm) through a PEEK union body. The water tube lead to a PEEK Tee body that connected to the main PTFE main channel (OD: 1587 μm, ID: 793 μm, L: 15 cm; Cole-Parmer, USA). This main channel was manually aligned coaxial to the fused silica capillary. As described in our previous work, the capillary alignment was the most delicate step.[14] In the main channel the two fluids were mixed and the formed NP suspension was collected in glass vials. The Reynolds number, *Re*, was calculated by estimating the velocities and characteristic lengths based on the inner cross section of the outer PTFE tube.

For the nanoprecipitation experiments, 10 mg of polymer (PEG-*b*-PCL, PEG-*b*-PLA, or PEG-*b*-PLGA) was dissolved in 1 mL of solvent (DMF, acetone, acetonitrile, THF, or DMSO; C_{poly} = 10 mg mL^{-1}). Water volumetric flow rates, Q_{water}, and the polymer solution volumetric flow rates, $Q_{polymer\ solution}$, ranged from 16 to 35 mL min^{-1} and from 80 to 174 μL min^{-1}, respectively. All flow-based experiments were performed with an R = 0.005, which was calculated as follows: $R = \frac{Q_{polysolution}}{Q_{water}}$. The flow rates corresponded to *Re* ranging from 428 to 937. The NP size and size distribution were measured via DLS. Every condition was performed at least in triplicate and NP size was given as mean ± standard error of the mean (SEM).

RESULTS AND DISCUSSION

Solvent Choice Influences NP Size. In a typical nanoprecipitation, an amphiphilic block copolymer—composed of a hydrophobic core-forming block, e.g., poly(DL-lactide) (PLA), poly(lactide-*co*-glycolide) (PLGA), or polycaprolactone (PCL), and a hydrophilic corona-forming block, e.g., poly(ethylene glycol) (PEG)—is dissolved in a solvent, such as acetonitrile. The block copolymer solution is mixed rapidly with water, a poor solvent for the core-forming block (Figure 1a). The transition from a favorable solvent to the nonfavorable solvent−water blend is described by a change in solvent quality, χ, for the hydrophobic block (Figure 1b).[43] This change in χ induces block copolymer assembly into nanoscale objects that become kinetically trapped (frozen) at a critical solvent quality, χ_c. Prior to χ_c the nanoscale objects can grow by unimer exchange and aggregate fusion.[17,40] The rate of change in χ depends on the time scale of mixing, τ_{mix}, and controls the extent of growth.[16] In this manner, nanoprecipitation transforms block copolymer solutions into stable, core−shell NPs with kinetically controlled size.[30,40]

To investigate the specific influence of the selected solvent on NP size, solutions of poly(ethylene glycol)-*block*-polylactide (PEG-*b*-PLA) were prepared in different water-miscible solvents. Core−shell NPs were produced from each block copolymer solution via nanoprecipitation. We prepared dilute solutions ($C_{poly} \leq$ 10 mg mL^{-1}) to limit the effect of polymer−polymer interactions in the organic phase. At the end of nanoprecipitation ϕ > 0.99, therefore, we assumed that the residual solvent fraction inside the NPs was negligible (Supporting Information Section S1). Batch nanoprecipitation of PEG-*b*-PLA formed spherical NPs with low dispersity in all solvents. Critically, the size of the formed NPs varied with the selected solvent, D_h = 65−101 nm ($Đ \approx$ 0.1) (Figure 1c). Nanoprecipitation with dimethylformamide (DMF) produced the smallest NPs, followed by acetone, acetonitrile, tetrahydrofuran (THF), and dimethyl sulfoxide (DMSO). NP size did not correlate with the HSP distance, *Ra*, or solvent viscosity (Supporting Information Section S2). This suggested that another physical parameter may explain the influence of solvent on NP size.

https://doi.org/10.1021/acs.macromol.2c00907
Macromolecules 2022, 55, 8040−8048

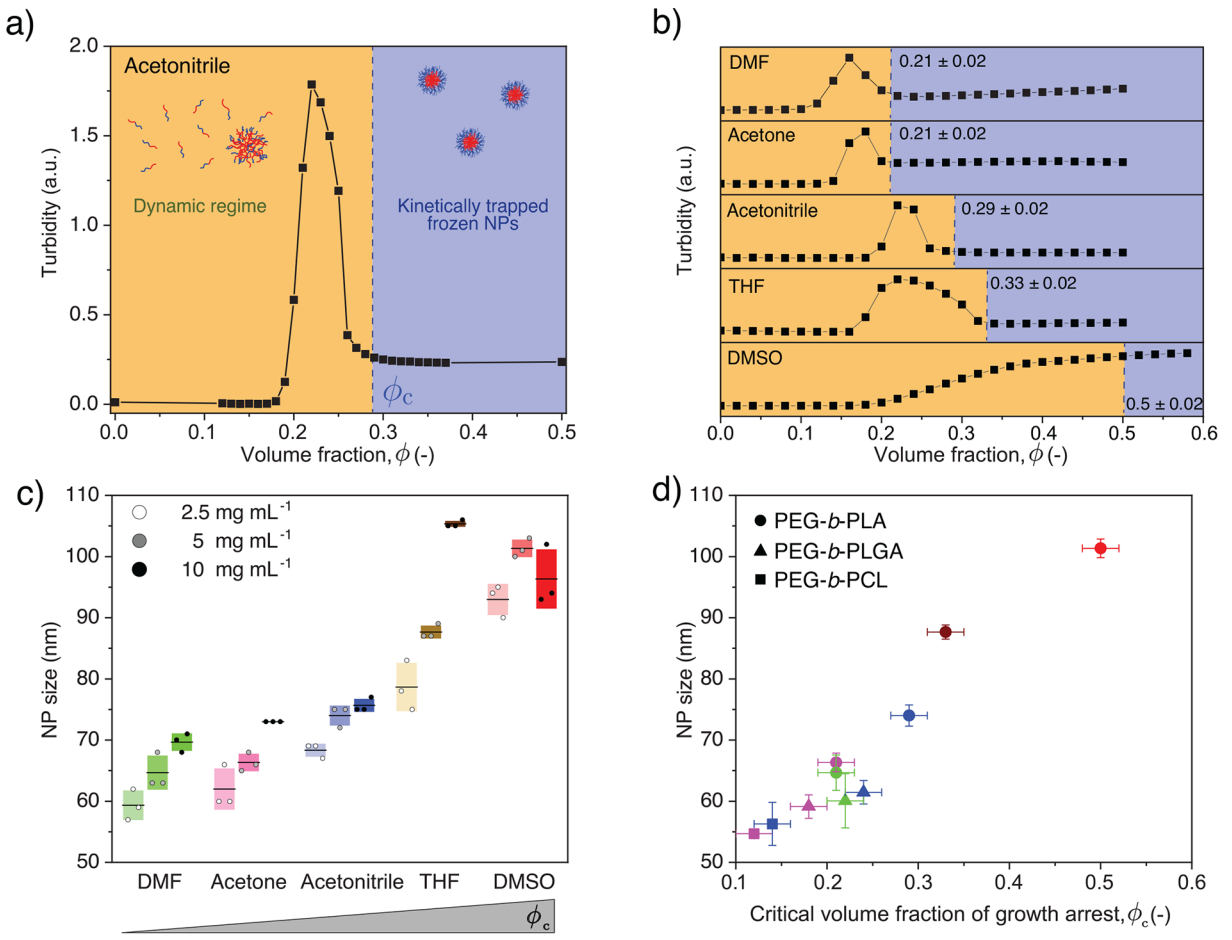

Figure 2. NP size scales with the solvent-dependent critical water fraction of growth arrest, ϕ_c. (a) The turbidity of a PEG-*b*-PLA solution in acetonitrile was measured for 0.01 $\Delta\phi$ increments in water volume fraction, ϕ. The suspension turbidity was negligible until $\phi \approx 0.19$, which marked the start of observable nanoassembly formation. Past $\phi \approx 0.19$, the turbidity varied with changes in ϕ, suggesting macroscopic nanoassembly dynamics. At a specific point, the turbidity did not change with further increases in ϕ. We defined this point as the critical water fraction of growth arrest, ϕ_c. (b) Turbidity curves for 10 mg mL^{-1} PEG-*b*-PLA solutions in different solvents (0.02 $\Delta\phi$ increments in water fraction) were used to calculate ϕ_c for each of the solvents tested: $\phi_{c,DMF} \approx \phi_{c,acetone} < \phi_{c,acetonitrile} < \phi_{c,THF} < \phi_{c,DMSO}$. (c) NP size following nanoprecipitation from 2.5, 5, and 10 mg mL^{-1} PEG-*b*-PLA for each of the solvents tested. Size increased with the measured ϕ_c for the different solvents. Data plotted as mean (black line) ± SD (colored boxes) for three independent experiments (symbols: 2.5 mg mL^{-1}, open circles; 5 mg mL^{-1}, gray circles; 10 mg mL^{-1}, solid circles). (d) NP size following nanoprecipitation from 5 mg mL^{-1} solutions of PEG-*b*-PLA (circles) in DMF, acetone, acetonitrile, THF, and DMSO correlated to the measured ϕ_c. Similar trends were observed for NPs formed from 10 mg mL^{-1} solutions of PEG-*b*-PLGA (triangles) and PEG-*b*-PCL (squares) in acetone, DMF, and acetonitrile. Data plotted as mean ± SD for three independent experiments. The x-error bars indicate the error in the ϕ_c measurements (±0.02).

Critical Water Fraction of Growth Arrest Dictates NP Size. We hypothesized that the choice of solvent defines a critical solvent−water composition at which the NPs became kinetically trapped (frozen). By setting a solvent-dependent freezing point, the solvent would influence NP size by allowing for differential extents of growth for the same mixing conditions.[40] To investigate whether a freezing point existed for the different solvents, we systematically increased the water fraction in the block copolymer solutions while monitoring polymer assembly. Block copolymer assembly was characterized by quantifying Rayleigh scattering (turbidity) of the solution as a function of the water fraction (Figure 2a).[22,44]

In a typical nanoprecipitation, the water fraction goes from 0.0 to beyond 0.9 on the milliseconds time scale, and the specific solvent−water composition at which the NPs become frozen is difficult to determine. To simulate block copolymer assembly during the early stages of mixing, we investigated small rates of change in water fraction ($\Delta\phi$ = 0.01−0.02 min^{-1}) from 0.0 to 0.5. For PEG-*b*-PLA in acetonitrile, the solution exhibited negligible turbidity until $\phi \approx 0.19$. Further increasing the water fraction induced a sharp rise in turbidity followed by a sharp decrease and a plateau at $\phi \approx 0.29$, beyond which no further changes in turbidity and NP properties were observed. We defined this value as the critical water fraction of growth arrest ϕ_c. Negligible turbidity below $\phi \approx 0.19$ suggested that the block copolymer chains existed as unimers or aggregates below the critical dimension for Rayleigh scattering (~25 nm).[42] Increasing the water fraction beyond the $\phi \approx 0.19$ induced assembly into structures that induced Rayleigh scattering.[22,23] The sharp increase and decrease in turbidity was attributed to the formation of dynamic assemblies (Supporting Information Section S3). The labile structures formed below ϕ_c could not be characterized reliably via DLS or TEM. Similar behavior has been reported for other block copolymers, such as PEG-*b*-PCL in acetonitrile and poly(*N*-isopropylacrylamide-*co*-dimethylacrylamide)-*block*-

https://doi.org/10.1021/acs.macromol.2c00907
Macromolecules 2022, 55, 8040−8048

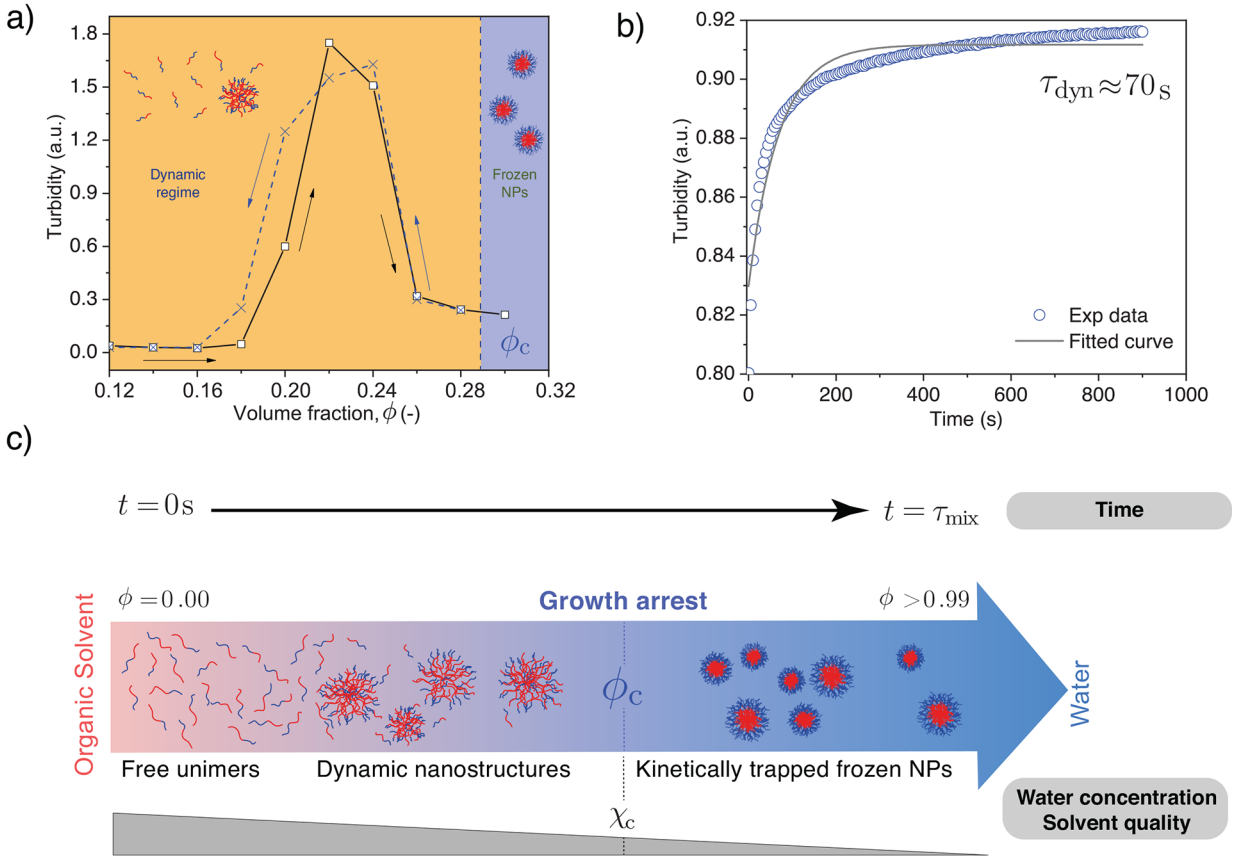

Figure 3. Dynamic turbidity measurements indicate dynamic assembly below ϕ_c. (a) The observed turbidity behavior as a function of ϕ was similar for increasing and decreasing $\Delta\phi$ increments in water fraction. This indicated that below ϕ_c nanoassembly properties depended on the specific water content and not on the direction of ϕ evolution. (b) Time-resolved turbidity of a 4 mg mL^{-1} PEG-*b*-PLA acetonitrile solution upon a step change in ϕ from 0.20 to 0.22 exhibited assembly dynamics on the time scale of seconds ($\phi_c \approx 0.28$; Supporting Information Section S5). The time scale of polymer rearrangement dynamics τ_{dyn} was quantified by fitting the curve to an empirical model. The model fit the turbidity change, ΔT, as a function of time, t, with a single-exponential function of the form $\Delta T \propto 1 - e^{-t/\tau_{dyn}}$.[47,49] Similar results were observed for other discrete changes in ϕ within the dynamic region ($\phi < \phi_c$). (c) In our proposed framework, dynamic polymer assemblies rearrange and grow through unimer exchange in the dynamic region. At ϕ_c, further growth is arrested and the NPs become kinetically trapped, as the solvent–water composition prevents further unimer exchange for $\phi > \phi_c$. Therefore, our hypothesis is that the extent of NP growth is controlled by the amount of time the system spends in the dynamic region, as dynamic rearrangement is slow relative to mixing ($\tau_{dyn} \gg \tau_{mix}$). This time is controlled by the solvent-dependent point of growth arrest, ϕ_c, and the mixing kinetics, rate of change in ϕ. These considerations are discussed further in the context of our *a priori* model.

poly(DL-lactide) in *N*,*N*-dimethylacetamide, and were described as unstable and swollen nanostructures.[23,45] Beyond ϕ_c, these assemblies formed frozen core–shell NPs. NPs collected at different solvent–water compositions beyond ϕ_c were colloidally stable.

All of the water-miscible solvents exhibited similar behavior with a dynamic region and a solvent-dependent ϕ_c (Figure 2b). ϕ_c increased sequentially: $\phi_{c,DMF} \approx \phi_{c,acetone} < \phi_{c,acetonitrile} < \phi_{c,THF} < \phi_{c,DMSO}$. In the case of DMSO, we did not observe a decrease in turbidity prior to ϕ_c; however, the turbidity reached a plateau at $\phi_c \approx 0.5$, and the NPs were colloidally stable beyond this point. Solutions of PEG-*b*-PLA (C_{poly} = 2.5, 5, and 10 mg mL^{-1}) in DMF, acetone, acetonitrile, THF, and DMSO were used to form NPs via batch nanoprecipitation. Interestingly, NP size correlated to the measured ϕ_c of the solvents (Figure 2c). In addition, NP size correlated to ϕ_c for solutions of PEG-*b*-PCL and PEG-*b*-PLGA (Figure 2d; Supporting Information Section S4). The data with different block copolymers indicated that the measured ϕ_c is a feature of the block copolymer and solvent pair. Overall, these experiments demonstrated that a solvent-dependent water composition, ϕ_c, exists beyond which the polymer assemblies become kinetically trapped (frozen).

Block Copolymer Aggregates Exhibit Slow Dynamics below ϕ_c. To explain how ϕ_c influenced NP size, we further investigated the dynamics of block copolymer assembly below the freezing point. The observed turbidity behavior was similar for increasing or decreasing ϕ (Figure 3a). This indicated that the dynamic region and ϕ_c were defined by the specific solvent and polymer pair and did not depend on the direction of ϕ evolution.[22,46] We then characterized the time scale of the dynamics, τ_{dyn}, in response to discrete changes in ϕ in the dynamic region using time-resolved turbidity measurements. The turbidity evolved over the course of seconds to hours, indicating slow rearrangement processes in the dynamic region ($\tau_{dyn} > 1$ s; Figure 3b; Supporting Information Section S5).[47,48] In addition, dynamic assemblies were unstable and prone to aggregation, whereas the nanoassemblies were colloidally stable beyond ϕ_c (Supporting Information Section S6). Depending on the storage conditions, frozen NPs remained stable over the course of weeks to months.

https://doi.org/10.1021/acs.macromol.2c00907
Macromolecules 2022, 55, 8040–8048

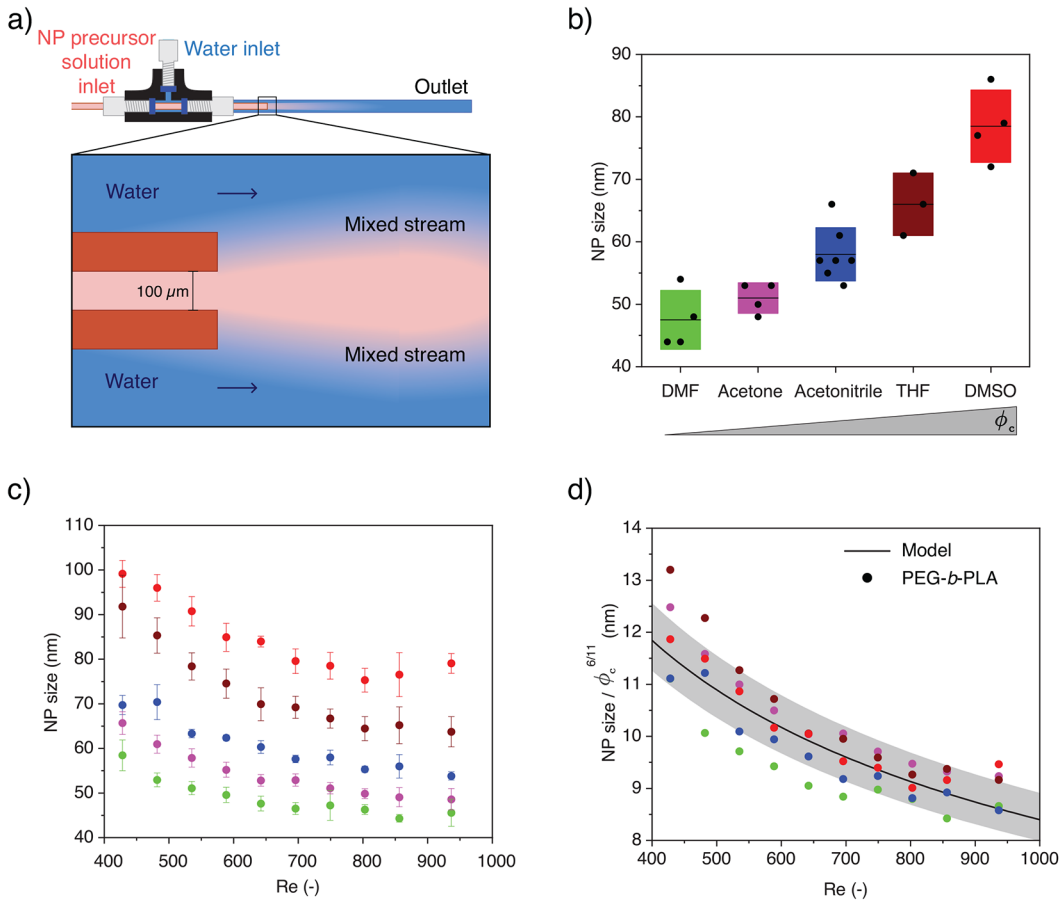

Figure 4. NP size scales with the solvent-dependent ϕ_c and mixing kinetics. (a) The mixing kinetics during nanoprecipitation were tuned by using a coaxial jet mixer (CJM) and controlling the solvent and nonsolvent flow velocities (and *Re*). In the CJM a stream containing a water-miscible solvent and a block copolymer (red) was mixed with a surrounding annulus of water (blue). NPs were formed from 10 mg mL^{-1} PEG-*b*-PLA in different solvents (R = 0.005). (b) NP size following nanoprecipitation in the CJM with constant mixing kinetics (Re = 749) correlated to ϕ_c. Data plotted as mean (black line) ± SD (colored box) for at least three independent experiments (black dots). (c) NP size following nanoprecipitation plotted as a function of *Re* (Re = 400−1000) correlated to ϕ_c across all mixing conditions. These data suggested universal scaling behavior for NP size based on solvent and mixing kinetics. Data plotted as mean ± SEM for at least three independent experiments. (d) NP size scaled by $\phi_c^{6/11}$ as a function of mixing conditions (*Re*) collapsed onto a single curve. The scaled data agreed with the scaling model (solid line) based on spinodal decomposition and dynamic growth. The shaded region shows the influence of the uncertainty in ϕ_c (±0.02) on the model.

Dynamic rearrangement of the formed aggregates below ϕ_c suggested a kinetic mechanism for the solvent-dependent NP size.[40] As the assembly dynamics were slow relative to the mixing kinetics ($\tau_{dyn} \gg \tau_{mix}$), we hypothesized that the amount of time the system spends in this dynamic region prior to reaching ϕ_c controlled the extent of aggregate growth or ripening (Figure 3c). This time depends on the rate of change in ϕ during nanoprecipitation, which is governed by the mixing kinetics and the boundary for growth arrest—the solvent-dependent ϕ_c. These considerations are further discussed in our *a priori* model based on spinodal decomposition and growth.

NP Size Depends on the Critical Water Fraction of Growth Arrest and the Mixing Kinetics. To study the combined effects of mixing kinetics and ϕ_c on NP size, we used a coaxial jet mixer (CJM) to nanoprecipitate block copolymer solutions under flow.[14,50] In the CJM, a central stream containing the water-miscible solvent and block copolymer was mixed with an outer stream of water (Figure 4a). The flow conditions in the CJM were varied to tune *Re*, and thereby τ_{mix} in the mixing channel.[13,14,51]

PEG-*b*-PLA was nanoprecipitated in the CJM for the different solvents by using the same flow conditions (Re = 749; Figure 4b). The NP size correlated to ϕ_c, supporting the central hypothesis that NP size depends on ϕ_c for a given τ_{mix}. To further investigate the influence of mixing kinetics on NP size, PEG-*b*-PLA solutions were nanoprecipitated in the CJM under varying flow conditions ($Re \approx$ 400−1000; Figure 4c). NP size decreased with increasing *Re* and NP size correlated to the measured ϕ_c for each solvent throughout the flow regime. We observed self-similar behavior for NP size as a function of *Re* across the different solvents, suggesting a scaling relation for NP size as a function of ϕ_c and *Re*.

Physical Model of Solvent Effects in Block Copolymer Nanoprecipitation. To explain the observed scaling behavior for NP size based on solvent and mixing kinetics, we developed a physical model of block copolymer assembly based on spinodal decomposition and growth up to the solvent-dependent freezing point, ϕ_c. A complete description of the physical model is included in the Supporting Information (Section S7). In the CJM, convective processes break up the polymer stream, and mixing between the polymer solution and water occurs within the smallest fluid element in which kinetic

https://doi.org/10.1021/acs.macromol.2c00907
Macromolecules 2022, 55, 8040−8048

energy is dissipated, the Kolmogorov length scale, which was estimated to be ~0.1−1 μm.[13,52] Following the work of Drese and colleagues, the main assumptions were that the initial stage of nanoprecipitation was governed by spinodal decomposition and that solvent controlled the extent of aggregate growth.[40,53] The system was described as block copolymers interacting in a solvent with time-varying χ. The initial state was taken as block copolymer unimers in pure solvent. The assembly of block copolymers into dynamic aggregates upon mixing with water was modeled via spinodal decomposition. Growth was allowed via unimer exchange up to ϕ_c. The time-dependent assembly process was modeled by using the Cahn−Hilliard equation[54]

$$\frac{\partial p}{\partial t} = \nabla \cdot \left[\xi M(p) \cdot \nabla \left(\frac{\partial f}{\partial p} - \lambda \Delta p \right) \right] \tag{1}$$

where p is the local aggregation number of block copolymers (Supporting Information, Section S8), $M(p)$ is the species mobility, f is the free energy per unit volume, and ξ and λ are constants. On the basis of the work of de Gennes, $M(p)$ for the initial phase of unimer aggregation scaled with p.[55,56] Following the work of Nose and Iyama, we estimated the free energy as

$$f(p) \approx \gamma_e N_1^{2/3} p^{2/3} \tag{2}$$

where γ_e is the effective interfacial energy between the hydrophobic core and the surroundings and N_1 is the degree of polymerization of the core forming block.[57] We combined eqs 1 and 2 to describe the evolution of the local aggregation number, p, as a function of time

$$\frac{\partial p}{\partial t} \propto C \gamma_e p^{4/15} \tag{3}$$

where C is a constant that depends on the physical parameters of the system.

The surface energy, γ_e, was related directly to the time-varying water fraction, $\phi(t)$.[58−61] As a first approximation, we assumed a linear increase in $\phi(t)$ up to ϕ_c.[58,59] The predicted NP size was calculated by using the dimension of the corona: NP size = $L_{NP} \propto N_2^{3/5} p^{1/5}$, where N_2 is the degree of polymerization of the corona forming block. Solving eq 3, with the above assumptions, from the initial condition to the freezing point, ϕ_c, we related NP size to ϕ_c and τ_{mix} or Re (using $\tau_{mix} \propto Re^{-11/8}$).[13,52]

$$\text{NP size} \propto \phi_c^{6/11} \tau_{mix}^{3/11} \propto \phi_c^{6/11} \text{Re}^{-3/8} \tag{4}$$

This model, based on spinodal decomposition and growth via unimer exchange up to ϕ_c, predicted that NP size scales with the mixing kinetics (τ_{mix} or Re) and the solvent-dependent critical water fraction of growth arrest (ϕ_c).

On the basis of the developed relationship, we scaled the experimental NP size by the measured $\phi_c^{6/11}$. The scaled NP size collapsed onto the predicted curve as a function of Re for all solvents (Figure 4d). In the tested regime, the scaling behavior supports the proposed physical model—dynamic aggregates grow in a similar process for all solvents, and growth is limited by the solvent-dependent ϕ_c (growth arrest). In this manner, the NP size was controlled by how fast the system reaches growth arrest. This can be tuned with τ_{mix} by varying the flow conditions of mixingor with ϕ_c by changing the solvent. The scaling law suggested how solvent controls NP size and provides useful guidelines to tailor the size of block copolymer NPs. It remains to be seen if these observed effects are limited to nonequilibrium (kinetically trapped systems), and further studies should explore other block copolymer−solvent systems as well as the role of solvent in equilibration nanoprecipitation.[62,63]

CONCLUSION

In this work, we explained how solvent affects NP size during block copolymer nanoprecipitation. Our proposed model suggests that dynamic polymer aggregates grow from the onset of assembly to growth arrest and that the water fraction for growth arrest is determined by the solvent. Turbidity measurements indicated dynamics below a critical water fraction and that kinetically trapped NPs were formed beyond this point. We defined this point as the critical water fraction of growth arrest, ϕ_c, which was measured for each solvent. The NP size correlated to the experimental ϕ_c for all solvents, block copolymers, and mixing kinetics tested in this work. We developed an *a priori* model, based on spinodal decomposition and growth via unimer exchange up to growth arrest, that described how NP size scales with ϕ_c and mixing kinetics. The experimental data for NP size collapsed onto the predicted curve from the model when scaled by ϕ_c. This supported the hypothesis that growth arrest ϕ_c controls NP size during nanoprecipitation. Overall, our study provides fundamental insight into the role of the solvent during the commonly used nanoprecipitation method and provides insight into another control variable in the design and engineering of block copolymer NPs.

ASSOCIATED CONTENT

Supporting Information

The Supporting Information is available free of charge at https://pubs.acs.org/doi/10.1021/acs.macromol.2c00907.

DLS and TEM measurements; HSP-related calculations; block copolymer turbidity, solvent turbidity, and time-resolved turbidity measurements; estimation of the timescale of block copolymer dynamics; full scaling law derivation; and supporting raw data (PDF)

AUTHOR INFORMATION

Corresponding Author

Mark W. Tibbitt − *Macromolecular Engineering Laboratory, Department of Mechanical and Process Engineering, ETH Zurich, 8092 Zurich, Switzerland;* orcid.org/0000-0002-4917-7187; Phone: +41 44 632 25 16; Email: mtibbitt@ethz.ch

Authors

Giovanni Bovone − *Macromolecular Engineering Laboratory, Department of Mechanical and Process Engineering, ETH Zurich, 8092 Zurich, Switzerland;* orcid.org/0000-0002-8508-0737

Lucien Cousin − *Macromolecular Engineering Laboratory, Department of Mechanical and Process Engineering, ETH Zurich, 8092 Zurich, Switzerland*

Fabian Steiner − *Macromolecular Engineering Laboratory, Department of Mechanical and Process Engineering, ETH Zurich, 8092 Zurich, Switzerland*

Complete contact information is available at: https://pubs.acs.org/10.1021/acs.macromol.2c00907

Notes

The authors declare no competing financial interest.

■ ACKNOWLEDGMENTS

This work was supported the Swiss National Science Foundation under project number 200021_184697 and start-up funds from ETH Zurich. The authors acknowledge Dr. M. Lucas-Droste and the Scientific Center for Optical and Electron Microscopy (ScopeM) of ETH Zurich for assistance with TEM imaging shown in the Supporting Information. The authors thank the Particle Technology Laboratory (Prof. Dr. S. E. Pratsinis, ETH Zurich) for generous access to their facilities. We also thank Prof. Dr. A. Gavriilidis and Prof. D. Marchisio for the fruitful discussions during the initial phase of the project.

■ REFERENCES

(1) Farokhzad, O. C.; Langer, R. Impact of Nanotechnology on Drug Delivery. *ACS Nano* **2009**, *3*, 16−20.
(2) Kamaly, N.; Xiao, Z.; Valencia, P. M.; Radovic-Moreno, A. F.; Farokhzad, O. C. Targeted polymeric therapeutic nanoparticles: design, development and clinical translation. *Chem. Soc. Rev.* **2012**, *41*, 2971−3010.
(3) Allen, T. M.; Cullis, P. R. Drug Delivery Systems: Entering the Mainstream. *Science* **2004**, *303*, 1818−1822.
(4) Appel, E. A.; Tibbitt, M. W.; Webber, M. J.; Mattix, B. A.; Veiseh, O.; Langer, R. Self-assembled hydrogels utilizing polymer−nanoparticle interactions. *Nat. Commun.* **2015**, *6*, 6295.
(5) Guzzi, E. A.; Bovone, G.; Tibbitt, M. W. Universal Nanocarrier Ink Platform for Biomaterials Additive Manufacturing. *Small* **2019**, *15*, 1905421.
(6) Bovone, G.; Guzzi, E. A.; Bernhard, S.; Weber, T.; Dranseikiene, D.; Tibbitt, M. W. Supramolecular Reinforcement of Polymer−Nanoparticle Hydrogels for Modular Materials Design. *Adv. Mater.* **2021**, 2106941.
(7) Ragelle, H.; Danhier, F.; Préat, V.; Langer, R.; Anderson, D. G. Nanoparticle-based drug delivery systems: a commercial and regulatory outlook as the field matures. *Expert Opin. Drug Delivery* **2017**, *14*, 851−864.
(8) Hickey, J. W.; Santos, J. L.; Williford, J.-M.; Mao, H.-Q. Control of polymeric nanoparticle size to improve therapeutic delivery. *J. Controlled Release* **2015**, *219*, 536−547.
(9) Park, K. Facing the truth about nanotechnology in drug delivery. *ACS Nano* **2013**, *7*, 7442−7447.
(10) Colombo, S.; Beck-Broichsitter, M.; Bøtker, J. P.; Malmsten, M.; Rantanen, J.; Bohr, A. Transforming nanomedicine manufacturing toward Quality by Design and microfluidics. *Adv. Drug Delivery Rev.* **2018**, *128*, 115−131.
(11) Suhara, M.; Miura, Y.; Cabral, H.; Akagi, D.; Anraku, Y.; Kishimura, A.; Sano, M.; Miyazaki, T.; Nakamura, N.; Nishiyama, A.; Kataoka, K.; Koyama, H.; Hoshina, K. Targeting ability of self-assembled nanomedicines in rat acute limb ischemia model is affected by size. *J. Controlled Release* **2018**, *286*, 394−401.
(12) Gref, R.; Minamitake, Y.; Peracchia, M.; Trubetskoy, V.; Torchilin, V.; Langer, R. Biodegradable long-circulating polymeric nanospheres. *Science* **1994**, *263*, 1600−1603.
(13) Lim, J.-M.; Swami, A.; Gilson, L. M.; Chopra, S.; Choi, S.; Wu, J.; Langer, R.; Karnik, R.; Farokhzad, O. C. Ultra-High Throughput Synthesis of Nanoparticles with Homogeneous Size Distribution Using a Coaxial Turbulent Jet Mixer. *ACS Nano* **2014**, *8*, 6056−6065.
(14) Bovone, G.; Guzzi, E. A.; Tibbitt, M. W. Flow-based reactor design for the continuous production of polymeric nanoparticles. *AIChE J.* **2019**, *65*, e16840.
(15) Nicolai, T.; Colombani, O.; Chassenieux, C. Dynamic polymeric micelles versus frozen nanoparticles formed by block copolymers. *Soft Matter* **2010**, *6*, 3111−3118.
(16) Johnson, B. K.; Prud'homme, R. K. Mechanism for Rapid Self-Assembly of Block Copolymer Nanoparticles. *Phys. Rev. Lett.* **2003**, *91*, 118302.
(17) Leibler, L.; Orland, H.; Wheeler, J. C. Theory of critical micelle concentration for solutions of block copolymers. *J. Chem. Phys.* **1983**, *79*, 3550−3557.
(18) Capretto, L.; Cheng, W.; Carugo, D.; Katsamenis, O. L.; Hill, M.; Zhang, X. Mechanism of co-nanoprecipitation of organic actives and block copolymers in a microfluidic environment. *Nanotechnology* **2012**, *23*, 375602.
(19) Mora-Huertas, C.; Fessi, H.; Elaissari, A. Polymer-based nanocapsules for drug delivery. *Int. J. Pharm.* **2010**, *385*, 113−142.
(20) Cheng, J.; Teply, B. A.; Sherifi, I.; Sung, J.; Luther, G.; Gu, F. X.; Levy-Nissenbaum, E.; Radovic-Moreno, A. F.; Langer, R.; Farokhzad, O. C. Formulation of functionalized PLGA-PEG nanoparticles for in vivo targeted drug delivery. *Biomaterials* **2007**, *28*, 869−876.
(21) Vangeyte, P.; Gautier, S.; Jérôme, R. About the methods of preparation of poly(ethylene oxide)-*b*-poly(ϵ-caprolactone) nanoparticles in water. *Colloids Surf., A* **2004**, *242*, 203−211.
(22) Yu, Y.; Zhang, L.; Eisenberg, A. Morphogenic Effect of Solvent on Crew-Cut Aggregates of Amphiphilic Diblock Copolymers. *Macromolecules* **1998**, *31*, 1144−1154.
(23) Jette, K. K.; Law, D.; Schmitt, E. A.; Kwon, G. S. Preparation and drug loading of poly(ethylene glycol)-*block*-poly(epsilon-caprolactone) micelles through the evaporation of a cosolvent azeotrope. *Pharm. Res.* **2004**, *21*, 1184−91.
(24) Lund, R.; Willner, L.; Pipich, V.; Grillo, I.; Lindner, P.; Colmenero, J.; Richter, D. Equilibrium chain exchange kinetics of diblock copolymer micelles: Effect of morphology. *Macromolecules* **2011**, *44*, 6145−6154.
(25) Galindo-Rodriguez, S.; Allémann, E.; Fessi, H.; Doelker, E. Physicochemical Parameters Associated with Nanoparticle Formation in the Salting-Out, Emulsification-Diffusion, and Nanoprecipitation Methods. *Pharm. Res.* **2004**, *21*, 1428−1439.
(26) Bilati, U.; Allémann, E.; Doelker, E. Development of a nanoprecipitation method intended for the entrapment of hydrophilic drugs into nanoparticles. *European Journal of Pharmaceutical Sciences* **2005**, *24*, 67−75.
(27) Liu, D.; Jiang, S.; Shen, H.; Qin, S.; Liu, J.; Zhang, Q.; Li, R.; Xu, Q. Diclofenac sodium-loaded solid lipid nanoparticles prepared by emulsion/solvent evaporation method. *J. Nanopart. Res.* **2011**, *13*, 2375−2386.
(28) Liu, D.; Cito, S.; Zhang, Y.; Wang, C.-F.; Sikanen, T. M.; Santos, H. A. A Versatile and Robust Microfluidic Platform Toward High Throughput Synthesis of Homogeneous Nanoparticles with Tunable Properties. *Adv. Mater.* **2015**, *27*, 2298−2304.
(29) Kalkowski, J.; Liu, C.; Leon-Plata, P.; Szymusiak, M.; Zhang, P.; Irving, T.; Shang, W.; Bilsel, O.; Liu, Y. In Situ Measurements of Polymer Micellization Kinetics with Millisecond Temporal Resolution. *Macromolecules* **2019**, *52*, 3151−3157.
(30) Pagels, R. F.; Edelstein, J.; Tang, C.; Prud'homme, R. K. Controlling and Predicting Nanoparticle Formation by Block Copolymer Directed Rapid Precipitations. *Nano Lett.* **2018**, *18*, 1139−1144.
(31) Liu, Y.; Kathan, K.; Saad, W.; Prud'homme, R. K. Ostwald ripening of β-carotene nanoparticles. *Phys. Rev. Lett.* **2007**, *98*, 036102.
(32) Nikoubashman, A.; Lee, V. E.; Sosa, C.; Prud'homme, R. K.; Priestley, R. D.; Panagiotopoulos, A. Z. Directed assembly of soft colloids through rapid solvent exchange. *ACS Nano* **2016**, *10*, 1425−1433.
(33) Chen, T.; Hynninen, A. P.; Prud'Homme, R. K.; Kevrekidis, I. G.; Panagiotopoulos, A. Z. Coarse-Grained Simulations of Rapid Assembly Kinetics for Polystyrene-b-poly(ethylene oxide) Copolymers in Aqueous Solutions. *J. Phys. Chem. B* **2008**, *112*, 16357−16366.

https://doi.org/10.1021/acs.macromol.2c00907
Macromolecules 2022, 55, 8040−8048

(34) Saad, W. S.; Prud'Homme, R. K. Principles of nanoparticle formation by flash nanoprecipitation. *Nano Today* **2016**, *11*, 212−227.
(35) Li, N.; Nikoubashman, A.; Panagiotopoulos, A. Z. Multi-scale simulations of polymeric nanoparticle aggregation during rapid solvent exchange. *J. Chem. Phys.* **2018**, *149*, 084904.
(36) Spaeth, J. R.; Kevrekidis, I. G.; Panagiotopoulos, A. Z. A comparison of implicit- and explicit-solvent simulations of self-assembly in block copolymer and solute systems. *J. Chem. Phys.* **2011**, *134*, 164902.
(37) Sato, T.; Takahashi, R. Competition between the micellization and the liquid-liquid phase separation in amphiphilic block copolymer solutions. *Polym. J.* **2017**, *49*, 273−277.
(38) He, X.; Schmid, F. Dynamics of spontaneous vesicle formation in dilute solutions of amphiphilic diblock copolymers. *Macromolecules* **2006**, *39*, 2654−2662.
(39) Ianiro, A.; Wu, H.; van Rijt, M. M.; Vena, M. P.; Keizer, A. D.; Esteves, A. C. C.; Tuinier, R.; Friedrich, H.; Sommerdijk, N. A.; Patterson, J. P. Liquid−liquid phase separation during amphiphilic self-assembly. *Nat. Chem.* **2019**, *11*, 320−328.
(40) Keßler, S.; Schmid, F.; Drese, K. Modeling size controlled nanoparticle precipitation with the co-solvency method by spinodal decomposition. *Soft Matter* **2016**, *12*, 7231−7240.
(41) He, X.; Schmid, F. Spontaneous Formation of Complex Micelles from a Homogeneous Solution. *Phys. Rev. Lett.* **2008**, *100*, 137802.
(42) Rabek, J. F. *Experimental Methods in Polymer Chemistry*; Wiley & Sons: New York, 1980; pp 861.
(43) Agrawal, A.; Saran, A. D.; Rath, S. S.; Khanna, A. Constrained nonlinear optimization for solubility parameters of poly(lactic acid) and poly(glycolic acid)—validation and comparison. *Polymer* **2004**, *45*, 8603−8612.
(44) Zhang, L.; Shen, H.; Eisenberg, A. Phase Separation Behavior and Crew-Cut Micelle Formation of Polystyrene-*b*-poly(acrylic acid) Copolymers in Solutions. *Macromolecules* **1997**, *30*, 1001−1011.
(45) Kohori, F.; Yokoyama, M.; Sakai, K.; Okano, T. Process design for efficient and controlled drug incorporation into polymeric micelle carrier systems. *J. Controlled Release* **2002**, *78*, 155−163.
(46) Shen, H.; Eisenberg, A. Morphological Phase Diagram for a Ternary System of Block Copolymer PS_{310}-*b*-PAA_{52}/Dioxane/H_2O. *J. Phys. Chem. B* **1999**, *103*, 9473−9487.
(47) Choucair, A. A.; Kycia, A. H.; Eisenberg, A. Kinetics of fusion of polystyrene-*b*-poly(acrylic acid) vesicles in solution. *Langmuir* **2003**, *19*, 1001−1008.
(48) Lund, R.; Willner, L.; Stellbrink, J.; Lindner, P.; Richter, D. Logarithmic chain-exchange kinetics of diblock copolymer micelles. *Phys. Rev. Lett.* **2006**, *96*, 068302.
(49) Chen, L.; Shen, H.; Eisenberg, A. Kinetics and Mechanism of the Rod-to-Vesicle Transition of Block Copolymer Aggregates in Dilute Solution. *J. Phys. Chem. B* **1999**, *103*, 9488−9497.
(50) Bovone, G.; Steiner, F.; Guzzi, E. A.; Tibbitt, M. W. Automated and Continuous Production of Polymeric Nanoparticles. *Frontiers in Bioengineering and Biotechnology* **2019**.
(51) Liu, D.; Zhang, H.; Fontana, F.; Hirvonen, J. T.; Santos, H. A. Current developments and applications of microfluidic technology toward clinical translation of nanomedicines. *Adv. Drug Delivery Rev.* **2018**, *128*, 54−83.
(52) Baldyga, J.; Bourne, J. A Fluid Mechanical Approach To Turbulent Mixing And Chemical Reaction Part II: Micromixing In The Light Of Turbulence Theory. *Chem. Eng. Commun.* **1984**, *28*, 243−258.
(53) Keßler, S.; Drese, K.; Schmid, F. Simulating copolymeric nanoparticle assembly in the co-solvent method: How mixing rates control final particle sizes and morphologies. *Polymer* **2017**, *126*, 9−18.
(54) Carter, W. C., Johnson, W. C., Eds.; *The Selected Works of John W. Cahn*; John Wiley & Sons, Inc.: Hoboken, NJ, 1998.
(55) de Gennes, P. G. Dynamics of fluctuations and spinodal decomposition in polymer blends. *J. Chem. Phys.* **1980**, *72*, 4756−4763.
(56) Otto, F.; E, W. Thermodynamically driven incompressible fluid mixtures. *J. Chem. Phys.* **1997**, *107*, 10177−10184.
(57) Nose, T.; Iyama, K. Micellization and relaxation kinetics of diblock copolymers in dilute solution based on A-W theory: I. Description of a model for core-corona type micelles. *Comput. Theor. Polym. Sci.* **2000**, *10*, 249−257.
(58) Kelley, E. G.; Smart, T. P.; Jackson, A. J.; Sullivan, M. O.; Epps, T. H. Structural changes in block copolymer micelles induced by cosolvent mixtures. *Soft Matter* **2011**, *7*, 7094−7102.
(59) Cooksey, T. J.; Singh, A.; Le, K. M.; Wang, S.; Kelley, E. G.; He, L.; Vajjala Kesava, S.; Gomez, E. D.; Kidd, B. E.; Madsen, L. A.; Robertson, M. L. Tuning Biocompatible Block Copolymer Micelles by Varying Solvent Composition: Core/Corona Structure and Solvent Uptake. *Macromolecules* **2017**, *50*, 4322−4334.
(60) Willner, L.; Poppe, A.; Allgaier, J.; Monkenbusch, M.; Richter, D. Time-resolved SANS for the determination of unimer exchange kinetics in block copolymer micelles. *Europhys. Lett.* **2001**, *55*, 667−673.
(61) Lund, R.; Willner, L.; Richter, D.; Dormidontova, E. E. Equilibrium chain exchange kinetics of diblock copolymer micelles: Tuning and logarithmic relaxation. *Macromolecules* **2006**, *39*, 4566−4575.
(62) Fesenmeier, D. J.; Park, S.; Kim, S.; Won, Y. Y. Surface mechanical behavior of water-spread poly(styrene)−poly(ethylene glycol) (PS−PEG) micelles at the air−water interface: Effect of micelle size and polymer end/linking group chemistry. *J. Colloid Interface Sci.* **2022**, *617*, 764−777.
(63) Nagarajan, R. "Non-equilibrium" block copolymer micelles with glassy cores: A predictive approach based on theory of equilibrium micelles. *J. Colloid Interface Sci.* **2015**, *449*, 416−427.

https://doi.org/10.1021/acs.macromol.2c00907
Macromolecules 2022, 55, 8040−8048